Environ Sci Pollut Res (2017) 24:21248–21255
DOI 10.1007/s11356-017-9766-y

RESEARCH ARTICLE

Heterogeneous reaction of NO_2 with soot at different relative humidity

Chong Han [1,2] · **Yongchun Liu** [1,3] · **Hong He** [1,3]

Received: 23 February 2017 / Accepted: 12 July 2017 / Published online: 22 July 2017

Abstract The influences of relative humidity (RH) on the heterogeneous reaction of NO_2 with soot were investigated by a coated wall flow tube reactor at ambient pressure. The initial uptake coefficient ($\gamma_{initial}$) of NO_2 showed a significant decrease with increasing RH from 7 to 70%. The $\gamma_{initial}$ on "fuel-rich" and "fuel-lean" soot at RH = 7% was $(2.59 \pm 0.20) \times 10^{-5}$ and $(5.92 \pm 0.34) \times 10^{-6}$, respectively, and it decreased to $(5.49 \pm 0.83) \times 10^{-6}$ and $(7.16 \pm 0.73) \times 10^{-7}$ at RH = 70%, respectively. Nevertheless, the HONO yields were almost independent of RH, with average values of (72 ± 3)% for the fuel-rich soot and (60 ± 2)% for the fuel-lean soot. The Langmuir-Hinshelwood mechanism was used to demonstrate the negative role of RH in the heterogeneous uptake of NO_2 on soot. The species containing nitrogen formed on soot can undergo hydrolysis to produce carboxylic species or alcohols at high RH, accompanied by the release of little gas-phase HONO and NO.

Keywords Soot · NO_2 · HONO · Relative humidity · Competitive adsorption

Responsible editor: Gerhard Lammel

✉ Hong He
honghe@rcees.ac.cn

[1] Research Center for Eco-Environmental Sciences, Chinese Academy of Sciences, Beijing 100085, China

[2] School of Metallurgy, Northeastern University, Shenyang 110819, China

[3] Center for Excellence in Urban Atmospheric Environment, Institute of Urban Environment, Chinese Academy of Sciences, Xiamen 361021, China

Introduction

Soot particles, which origin from the incomplete combustion of fossil and biomass fuels, are ubiquitous in the atmosphere. With an average emission inventory of 8–24 Tg of carbon per year, soot may account for ~10–15% of the total atmospheric aerosol mass (Penner and Eddleman 1993). Soot can provide a large specific surface area for the heterogeneous reactions, leading to changes in the atmospheric compositions by the chemical reactions of active species such as HO, O_3, NO_2, NO_3, N_2O_5, HNO_3, and H_2SO_4 (Ammann et al. 1998; Arens et al. 2001; Bertram et al. 2001; Gerecke et al. 1998; McCabe and Abbatt 2009; Khalizov et al. 2010; Kleffmann and Wiesen 2005; Lelièvre et al. 2004a, b; Saathoff et al. 2001; Salgado Muñoz and Rossi 2002; Stadler and Rossi 2000; Zhang and Zhang 2005). In particular, the chemical conversion of NO_2 to HONO on soot has attracted extensive attention as a possible source of HONO in the past years, thus affecting the oxidation capacity of the atmosphere.

Many studies have measured the uptake coefficient (γ) of NO_2 and HONO yield on various soot including fuel combustion soot (*n*-hexane (Aubin and Abbatt 2007; Lelièvre et al. 2004b; Prince et al. 2002; Stadler and Rossi 2000), decane (Aubin and Abbatt 2007; Stadler and Rossi 2000), toluene (Kleffmann et al. 1999; Lelièvre et al. 2004b), and diesel (Kleffmann et al. 1999)), commercially available soot such as Degussa FW2 and Printex (Kleffmann et al. 1999), and spark discharge soot from graphite electrodes (Ammann et al. 1998; Kalberer et al. 1999a, b). The values of γ varied greatly from 10^{-1} to 10^{-8} as well as HONO yields were in a wide range of 0–100% (Ammann et al. 1998; Arens et al. 2001; Aubin and Abbatt 2007; Kalberer et al. 1999a; Khalizov et al.

2010; Kleffmann et al. 1999; Lelièvre et al. 2004b; Prince et al. 2002; Stadler and Rossi 2000), which may depend on the reaction conditions such as source of soot, structure and composition of soot, NO_2 concentration, and relative humidity (Prince et al. 2002).

The HONO generation from the reaction of NO_2 with H_2O adsorbed on glass, Pyrex, and Teflon has been observed, suggesting a following possible reaction pathway (Finlayson-Pitts et al. 2003),

$$2NO_2 + H_2O \rightarrow HONO + HNO_3 \quad R1$$

However, this mechanism is not applicable to the uptake of NO_2 on the soot surface, where HNO_3 was not detected as a product and the HONO yield was usually higher than 50%. This suggests that soot provides reactive surface sites for the HONO formation via a redox process (R2) (Kleffmann and Wiesen 2005; Stadler and Rossi 2000),

$$NO_2 + R_{re} \rightarrow HONO + R_{ox} \quad R2$$

Soot contains various polar oxygen-containing functional groups such as C–O, C = O, OH, and COOH (Cain et al. 2010; Daly and Horn 2009; Han et al. 2012a, b), which may become the active adsorption sites of H_2O. The adsorbed H_2O may block some adsorptive or reactive sites of NO_2, and thus decreasing the NO_2 uptake and HONO formation. As observed by Kalberer et al. (1999a), above the relative humidity of 40%, the HONO production decreased with increasing relative humidity due to competitive adsorption of H_2O on the soot surface. Nevertheless, Kleffmann et al. (1999) found that the HONO yield increased continuously with increasing relative humidity, reaching an almost constant value of 50% at high relative humidity (>60%). In contrast, within the relative humidity range of 0–80%, Arens et al. (2001) reported that relative humidity cannot affect the formation of HONO. Therefore, the roles of H_2O in the reaction of NO_2 to HONO on soot should be further investigated. In order to obtain reliable kinetic parameters, it is required to measure the reaction kinetics of NO_2 with soot at ambient relative humidity.

In this work, soot was produced by combusting *n*-hexane under controlled conditions. The uptake experiments of NO_2 on soot were performed using a flow tube reactor coupled to a NO_x analyzer at ambient pressure. The uptake coefficients of NO_2 and HONO yields were measured as a function of relative humidity (RH). Langmuir-Hinshelwood mechanism was employed to explain the competition role of H_2O in the NO_2 uptake on soot. The changes in the compositions of soot were analyzed by in situ attenuated total internal reflection infrared (ATR-IR) spectra. The role of RH in the release of HONO on the NO_2-treated soot was also examined.

Experimental sections

Soot production

Soot samples were produced by combusting *n*-hexane (AR, Sinopharm Chemical Reagent Lo., Ltd) in a co-flow diffusion burner as described in detail elsewhere (Han et al. 2012a, b). This burner basically consisted of a diffusion flame maintained by an airflow. The fuel was fed by a cotton wick extending into the liquid fuel reservoir. The airflow was a mixture of high purity O_2 and N_2, and the volume ratio of O_2 to N_2 was exactly controlled by mass flow meters. The fuel/oxygen ratio was expressed as the molar ratio of the consumed fuel to the introduced oxygen during the combustion process. The samples produced at a relatively high fuel/oxygen ratio (0.18) were defined as "fuel-rich" soot, whereas the samples generated at a relatively low fuel/oxygen ratio (0.10) were defined as "fuel-lean" soot. At the burner exit, the collection of soot on the inner walls of a quartz tube was quickly completed within 20 s, which avoided a significant removal of organic carbon on soot due to the increase in the temperature of the tube. And then, the tube coated with soot was quickly transferred to the reactor, where a N_2 flow was introduced to avoid the aging of soot by the oxidizing species. With nitrogen Brunauer-Emmett-Teller (BET) physisorption analysis (Quantachrome Autosorb-1-C), the specific surface area of soot was measured to be 52.0 m^2/g, which was used to calculate the mass-independent uptake coefficient.

Flow tube reactor

The heterogeneous reaction of NO_2 with soot was performed in a horizontal cylindrical coated wall flow tube reactor at ambient pressure. The temperature was maintained at 298 K by circulating water through the outer jacket of the flow tube reactor (34 cm length and 1.6 cm inner diameter). The quartz tube (20 cm length, 1.0 cm inner diameter, and 1.4 cm outside diameter) coated with soot samples was located at the center of the reactor. NO_2 standard gas (50 ppmv in N_2, Beijing Huayuan Gases Inc.) and high purity N_2 (99.99%, Beijing AP BEIFEN Gases Inc.) were used as received. With high purity N_2 as carrier gas, the total flow introduced into the reactor was 930 ml min^{-1}, which ensured a laminar regime in the sample tube. NO_2 was introduced into the flow tube through a movable injector with 0.6 cm outside diameter, and its concentration was 160 ppb. During the reaction processes of NO_2 with soot, the NO_2 and NO concentrations were measured by a chemiluminescence analyzer (THERMO 42i). A quartz tube (10 cm length and 1.0 cm inner diameter) filled with 1.0 g Na_2CO_3 was introduced to trap the formed HONO between the exit of the reactor and the analyzer, since HONO was also detected as NO_2 by the analyzer (Monge et al. 2010). NO and NO_2 together with HONO were detected using a

bypass tube, whereas only NO and NO_2 were measured using this Na_2CO_3 tube. Thus, the HONO concentration was indirectly obtained as the difference of the NO_2 signal without and with the Na_2CO_3 tube in the sampling line. RH was adjusted in the range of 7–70% by varying the ratio of dry N_2 to wet N_2, and it was measured using a hygrometer (Center 314). The trapping efficiency of HONO by the Na_2CO_3 tube was higher than 99% at different RH over 1.0 h for a 200 ppb HONO flow (Liu et al. 2015). The NO_2 uptake and HONO decomposition on the quartz tube were negligible during the control experiments. According to the detection limit (0.4 ppb) of the NO_x analyzer, the systematic uncertainties of the NO_2 signal should be less than 7%, which depended on the concentrations of NO_2.

Uptake coefficient

The uptake behavior of NO_2 on soot can be described by a pseudo-first-order reaction (Monge et al. 2010). As shown in the following equation, the pseudo-first-order rate constant (k_{obs}) was proportional to the geometric uptake coefficient (γ),

$$\frac{\ln\left(C_0/C_t\right)}{t} = k_{\text{obs}} = \frac{\gamma < c >}{2r_{tube}}, \quad (1)$$

where C_0 and C_t are the NO_2 concentration at exposure time 0 and t, respectively; $<c>$ and r_{tube} are the NO_2 average molecular velocity and the inner radius of sample tube, respectively. Since the diffusion of NO_2 into underlying layers of soot samples may happen, γ was a mass-dependent parameter and exhibited a linear increase in the soot mass range of 0.3–2.0 mg. Therefore, the mass-independent uptake coefficient (γ_{BET}) was calculated using Eq. 2,

$$\gamma_{\text{BET}} = \frac{S_{geom} \times \gamma_{geom}}{S_{\text{BET}} \times m_{soot}}, \quad (2)$$

where S_{geom} is the geometric area of the quartz tube coated with soot, S_{BET} is the BET surface area of soot, and m_{soot} is the soot mass. The Cooney-Kim-Davis (CKD) method was used to correct the gas-phase diffusion limitations for γ_{geom} calculations (Cooney et al. 1974; Murphy and Fahey 1987), which has been widely described in previous studies (Monge et al. 2010; Ndour et al. 2009; Zelenay et al. 2011). According to Eqs. 1 and 2, initial uptake coefficients ($\gamma_{initial}$) of NO_2 on soot were determined by averaging the NO_2 signal within the first 1.0 min during the reaction with soot, because the data was automatically recorded every minute by NO_x analyzer.

Analysis of soot surface compositions

The in situ attenuated total internal reflection infrared (ATR-IR) spectra during the reaction of NO_2 with soot were recorded using a Fourier transform infrared (FT-IR) spectrometer (NEXUS 6700). Soot produced by the *n*-hexane flame was directly deposited on the ZnSe crystal of the ATR-IR cell, which was sealed with quartz glass. Soot was purged by 100 ml min^{-1} N_2 for 1 h at 298 K. Subsequently, a mixture of NO_2 and N_2 with a total flow rate of 100 ml min^{-1} was introduced into ATR-IR cell. A high NO_2 concentration (5 ppm) was used to obtain better ATR-IR spectra signals. The spectra of soot were recorded (100 scans, 4 cm^{-1} resolution) using the unreacted soot surface as reference. The experiments were performed at 298 K under ambient pressure.

Results and discussion

NO_2 uptake and HONO formation at different RH

Figure 1 shows the temporal changes of NO_2 and HONO concentrations in the reaction of NO_2 with soot. Upon exposure to soot, there was a clear time-dependent loss of NO_2 with a significant initial uptake (Fig. 1a). Due to the consumption of active sites, the deactivation of soot occurred quickly. When NO_2 was isolated from soot by moving the injector outside the reaction region, the NO_2 desorption was not observed, indicating that the reactive uptake should be the main contributor to the loss of NO_2. Figure 1b shows that HONO was always released to the gas phase as long as NO_2 was consumed on soot. Moreover, coupled with initial NO_2 uptake, the HONO concentration reached the maximum value.

Soot surface has various oxygen-containing species such as ethers, ketones, lactones, and anhydrides (Cain et al. 2010; Daly and Horn 2009; Han et al. 2012a, b), which may become so-called primary adsorption centers to H_2O. Uptake of H_2O on soot has been observed by a Knudsen reactor connected with a mass spectrometer (Seisel et al. 2004). Therefore, H_2O may have significant influences on the heterogeneous uptake reaction of NO_2 on soot. As shown in Fig. 1, compared to those at RH = 7%, NO_2 exhibited a lower initial uptake as well as HONO reached a lower maximum value at RH = 70%, remaining to continue over a following interval of tens of minutes. The integrated amounts of the lost NO_2 and the formed HONO within 90 min decreased from 1.59×10^{17} and 1.21×10^{17} molecules at RH = 7% to 1.06×10^{17} and 8.05×10^{16} molecules at RH = 70%, respectively. Based on BET area of soot, the number of NO_2 lost per unit specific soot surface area was calculated to decrease from 3.06×10^{14} molecules cm^{-2} at RH = 7% to 2.04×10^{14} molecules cm^{-2} at RH = 70% within 90 min. These values roughly corresponded to the number of surface reactive sites consumed per unit specific soot surface area. This confirms that H_2O has negative effects on the NO_2 uptake and HONO formation on soot.

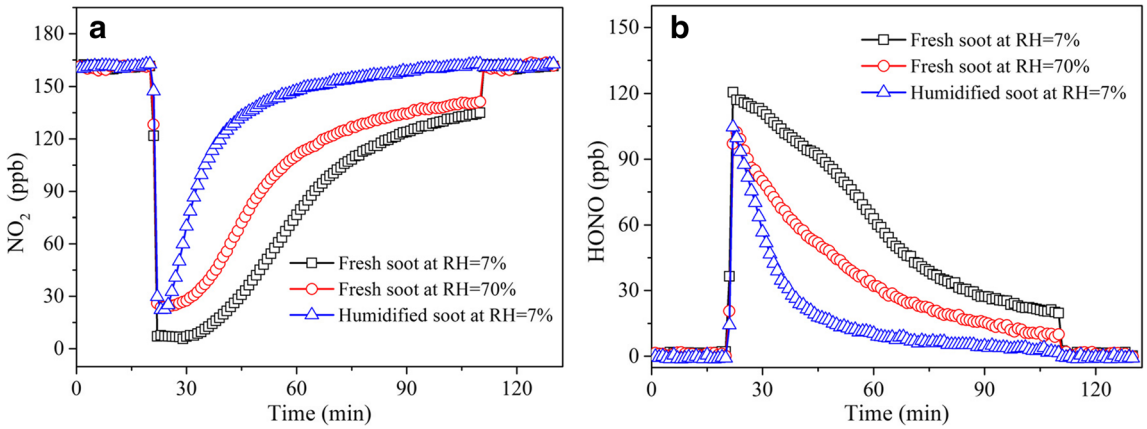

Fig. 1 Temporal changes of NO_2 uptake (**a**) and HONO formation (**b**) on fresh "fuel-rich" soot at RH = 7% and 70% and humidified "fuel-rich" soot (soot was exposed to wet N_2 for 30 min at 25 °C) at RH = 7%

To further identify the negative role of H_2O, a second set of experiments were performed in which soot that had been exposed to wet N_2 for 30 min was then exposed to NO_2 at RH = 7%. Compared to that on fresh soot at RH = 7%, NO_2 concentration on soot humidified by wet N_2 had a faster asymptotic recovery after the initial uptake, accompanied by a faster decrease of HONO concentration after reaching the maximum value. These results indicate that absorbed H_2O leads to the decreases in the reactivity of soot toward NO_2, which may be related to the restructuring of soot. Soot can collapse and become more compact due to pore condensation of H_2O at high RH (Ma et al. 2013; Martin et al. 2013; Mikhailov et al. 2006), inhibiting the diffusion of NO_2 into the pore space of soot. Thus, some reactive sites available for NO_2 uptake and HONO formation on soot can be blocked by absorbed H_2O.

Figure 2 shows the initial uptake coefficient ($\gamma_{initial}$) of NO_2 on fresh soot as a function of RH. The errors represent the standard deviations based on three independent experiments. The $\gamma_{initial}$ exhibited the inverse dependence on RH. The $\gamma_{initial}$ on fuel-rich soot decreased from $(2.59 \pm 0.20) \times 10^{-5}$ at RH = 7% to $(5.49 \pm 0.83) \times 10^{-6}$ at RH = 70%. The $\gamma_{initial}$ on fuel-lean soot decreased from $(5.92 \pm 0.34) \times 10^{-6}$ to $(7.16 \pm 0.73) \times 10^{-7}$ with increasing the RH from 7 to 70%. The decrease of $\gamma_{initial}$ with RH can be ascribed to the competitive adsorption between H_2O and NO_2 on soot. Popovicheva et al. (2008) found that the adsorbed H_2O on soot continuously increased with RH from 0 to 70%. The $\gamma_{initial}$ $(3.6 \pm 2.0) \times 10^{-4}$ of H_2O on soot was significantly larger than that of NO_2 as mentioned above (Seisel et al. 2004), meaning that the adsorption of H_2O is preferred over NO_2. This can well explain a decrease of $\gamma_{initial}$ of NO_2 with RH. In addition, it was noticed that the reactivity of fuel-lean soot toward NO_2 was significantly lower than that of fuel-lean soot. It has been reported that the reactivity of soot toward NO_2 linearly depended on the contents of organic carbon in soot, which decreased with decreasing the fuel/oxygen ratio (Han et al. 2013b). As described in the "Experimental section", N_2 was used as the carrier gas without O_2. The composition of soot almost remained unchanged after the exposure to O_2 in the dark (Han et al. 2012b), suggesting that O_2 may have a slight effect on the uptake of NO_2 on soot. The values reported here should be the upper limit for the reaction of NO_2 with soot.

Figure 3 summarizes the HONO yield when NO_2 reacted with fresh soot at different RH. The HONO yield was defined as the ratio of integrated HONO formation amount to integrated NO_2 loss amount on soot. In the RH range of 7–70%, the HONO yields almost remained unchanged. The average HOHO yield was (72 ± 3)% and (60 ± 2)% for fuel-rich and fuel-lean soot, respectively. This suggests that H_2O is not limiting for the HONO generation on soot, since it may be already in large excess over the ppb NO_2 at low RH. In fact, the formation of HONO by the reaction of NO_2 with soot under dry conditions has been observed (Al-Abadleh and Grassian 2000; Aubin and Abbatt 2007; Lelièvre et al. 2004b; Stadler and Rossi 2000).

The average integrated HONO formation amount on fuel-rich soot at RH = 30–70% was calculated to be

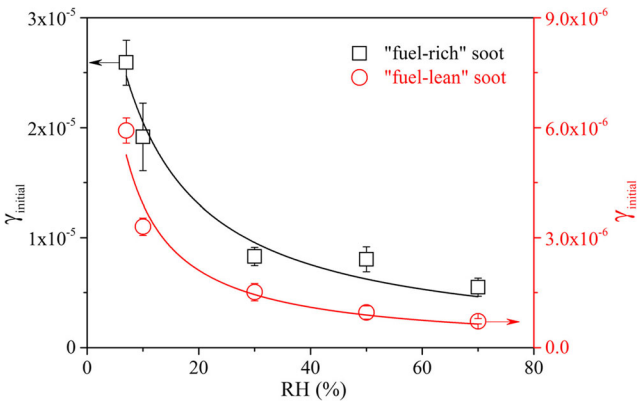

Fig. 2 Plots of $\gamma_{initial}$ of NO_2 on fresh "fuel-rich" and "fuel-lean" soot versus RH. The *black* and *red solid* lines are the fitting curve using Eq. 10

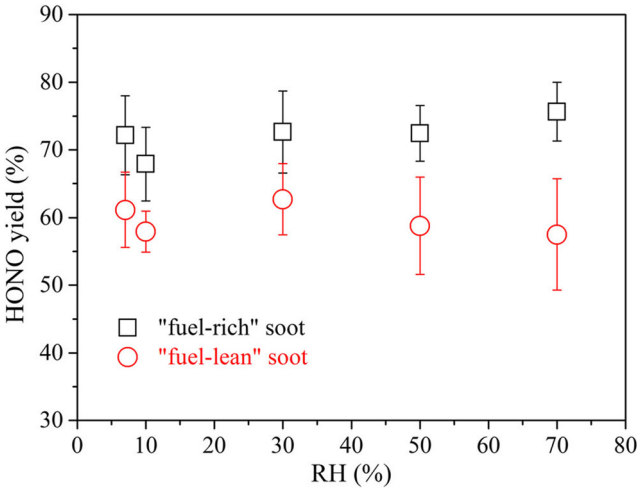

Fig. 3 Plots of the HONO yield on fresh "fuel-rich" and "fuel-lean" soot versus RH

1.75×10^{12} molecules cm^{-2} min^{-1}. A typical aerosol surface concentration was reported to be 10^3 μm^2 cm^{-3} in the urban atmosphere (Hueglin et al. 2005; Wehner and Wiedensohler 2003), and the mass of soot may reach an upper limit of 10–15% of the total atmospheric aerosols (Khalizov et al. 2010; Penner and Eddleman 1993). Thus, in the RH range of 30–70%, the formation rate of HONO by the reaction of NO_2 with soot in aerosols was estimated to be 4–6 ppt h^{-1}. This value should be obviously larger than the average HONO formation rate in the typical atmospheric lifetime (several days) of soot, because the reaction kinetics of NO_2 with soot quickly slowed down due to the consumption of the reactive sites on soot (Fig. 1a). Additionally, the NO_2 concentration and the soot mass proportion used to determine the HONO formation rate were larger than the corresponding average atmospheric levels, which may cause an overestimation of the HONO formation rate.

Langmuir-Hinshelwood mechanism analysis

Assuming that the uptake of NO_2 on soot follows the Langmuir-Hinshelwood mechanism, NO_2 is in rapid equilibrium between the gas phase and the soot surface, and the reaction takes place between the adsorbed species. If the surface reaction is the rate-limiting step, the pseudo-first-order reaction rate (v) of NO_2 can be written as:

$$-\frac{d[NO_2]_{ads}}{dt} = v = k_1[NO_2]_{ads} = k_1[S]_T\theta_{NO_2} \quad (3)$$

where t is the reaction time, $[NO_2]_{ads}$ is the adsorbed NO_2, k_1 is the pseudo-first-order reaction rate coefficient, $[S]_T$ is the total number of surface adsorption sites, and θ_{NO_2} is the fraction of the sites occupied by NO_2. If the adsorption of NO_2 on soot can be described by the Langmuir isotherm, θ_{NO_2} is given by Eq. 4 (Liu et al. 2015),

$$\theta_{NO_2} = \frac{K_{NO_2}[NO_2]_g}{1 + K_{NO_2}[NO_2]_g + K_{H_2O}[H_2O]_g}, \quad (4)$$

where K_{NO_2} and K_{H_2O} are the Langmuir adsorption constant for NO_2 and H_2O, respectively, and $[NO_2]_g$ and $[H_2O]_g$ are the concentrations of NO_2 and H_2O, respectively. By substituting Eq. 4 into Eq. 3, the following equation is obtained:

$$v = \frac{k_1[S]_T K_{NO_2}[NO_2]_g}{1 + K_{NO_2}[NO_2]_g + K_{H_2O}[H_2O]_g} \quad (5)$$

Thus, the pseudo-first-order rate coefficient is written as:

$$k_{1,NO_2} = \frac{k_1[S]_T K_{NO_2}}{1 + K_{NO_2}[NO_2]_g + K_{H_2O}[H_2O]_g} \quad (6)$$

By inserting Eq. 7 and Eq. 8 into Eq. 6,

$$k_{1,NO_2} = \frac{\gamma\langle c_{NO_2}\rangle}{2r_{tube}} \quad (7)$$

$$[H_2O] = \frac{P^0_{H_2O}[RH]}{RT} \quad (8)$$

The dependence of γ on RH can be described by Eq. 9,

$$\gamma = \frac{\left(2r_{tube}\Big/\langle c_{NO_2}\rangle\right)k_1[S]_T K_{NO_2}}{1 + K_{NO_2}[NO_2]_g + \dfrac{K_{H_2O}P^0_{H_2O}[RH]}{RT}} \quad (9)$$

Because the uptake experiments were performed at a constant NO_2 concentration, Eq. 9 can be simplified to Eq. 10,

$$\gamma = \frac{a}{b + c[RH]}, \quad (10)$$

where $a = (2r_{tube}/\langle c_{NO_2}\rangle)k_1[S]_T K_{NO_2}$, $b = 1 + K_{NO_2}[NO_2]_g$, and $c = \frac{K_{H_2O}P^0_{H_2O}}{RT}$. As shown in Fig. 2, the data of $\gamma_{initial}$ as a function of RH was fitted using Eq. 10. The well-fitting results suggest that the Langmuir-Hinshelwood mechanism can satisfactorily describe the effects of RH on the uptake coefficients. The resulting equation for fuel-rich and fuel-lean soot is Eqs. 11 and 12, respectively.

$$\gamma_{initial} = \frac{1.87 \times 10^{-4}}{3.92 + 0.52[RH]} \quad (11)$$

$$\gamma_{initial} = \frac{6.57 \times 10^{-5}}{2.48 + 1.43[RH]} \quad (12)$$

According to Eqs. 11 and 12, the $\gamma_{initial}$ for fuel-rich and fuel-lean soot at RH = 0% was extrapolated to be 4.77×10^{-5}

and 2.65×10^{-5}, respectively. The $\gamma_{initial}$ value at RH = 0% in this work was close to the reported values of $\gamma_{initial}$, from 3.9×10^{-5} to 5×10^{-5} for NO_2 on hexane soot under dry conditions (Al-Abadleh and Grassian 2000; Aubin and Abbatt 2007). The typical RH generally varied at 20–90% in the troposphere. As found in this work, the $\gamma_{initial}$ of NO_2 on soot decreased with increasing RH. Thus, the $\gamma_{initial}$ measured under dry conditions should result in an overestimated uptake ability of soot toward NO_2. It should be pointed out that the NO_2 uptake coefficients would decrease as the active sites on soot were continuously consumed with exposure time. Soot may be also aged by various processes in the atmosphere such as the oxidization and the coating with organics, which may affect the kinetics of NO_2 on soot at different RH.

Hydrolysis of species containing nitrogen formed on soot

Besides gaseous HONO, surface species containing nitrogen have been confirmed during the heterogeneous reaction of NO_2 with soot (Akhter et al. 1984; Han et al. 2013a; Kirchner et al. 2000). The in situ ATR-IR spectra were used to investigate the temporal changes in the functional groups of soot. The unreacted soot surface was taken as the reference background spectrum. To obtain better IR signal, ATR-IR spectra of soot were recorded at a higher NO_2 concentration (5 ppm). N_2O_4 may be involved in the reactions at high NO_2 concentrations. According to Akhter et al. (1984) and Sosedova et al. (2011), the equilibrium between NO_2(g) and NO_2(ads)/N_2O_4(ads) was first built before the reaction with soot. The pseudo-first-order rate coefficient at 5 ppm NO_2 will be orders of magnitude smaller than that at 160 ppb NO_2, whereas there are similar products in the reactions of soot with 160 ppb NO_2 and 5 ppm NO_2 (Han et al. 2013a).

As shown in Fig. 4, ATR-IR spectra exhibited significant changes during the reaction of soot with NO_2. The intensities of peaks at 1633, 1550, 1505, 1325, 1280, 900, 850, and 783 cm^{-1} increased with the time. The peaks at 1633 and 1280 cm^{-1} were attributed to R-ONO (Akhter et al. 1984; Al-Abadleh and Grassian 2000; Kirchner et al. 2000). Two peaks at 1550 and 1325 cm^{-1} were ascribed to aliphatic R-NO_2, while the band around 1505 cm^{-1} was assigned to aromatic Ar-NO_2 (Akhter et al. 1984; Al-Abadleh and Grassian 2000; Kirchner et al. 2000). Three peaks at 900, 850, and 783 cm^{-1} were related to R-ONO_2/R-ONO (Al-Abadleh and Grassian 2000). These results suggest that the species containing nitrogen were formed on the soot surface, which can be a reason of the fact that the HONO yield is always less than 100% (Fig. 3). In addition, the intensities of two bands at 3276 and 3038 cm^{-1} obviously decreased, which was related to the consumption of alkyne and aromatic C-H, respectively.

The soot aged by NO_2 (5 ppm) was exposed to a constant relative dry N_2 flow (RH = 7%) to promote desorption of species from the soot surface. Once the changes of ATR-IR spectra was not observed, the aged soot was exposed to a wet N_2 flow (RH = 70%). The aged soot was taken as the reference background spectrum. Figure 5 shows the changes of ATR-IR spectra when soot aged by NO_2 was exposed to wet N_2 at 30 min. Two negative peaks at 872 and 806 cm^{-1} resulted from the decrease of R-ONO_2/R-ONO (Al-Abadleh and Grassian 2000), confirming the hydrolysis of species containing nitrogen. The peak at 1375 cm^{-1} was assigned to carboxylic species or alcohols, which resulted from the hydrolysis of lactone or anhydride species, as described by the negative peak at 1738 cm^{-1} (Daly and Horn 2009). The OH in H_2O was also detected at 1622 and 3448 cm^{-1}, suggesting the presence of H_2O adsorbed on the soot surface. It was noticeable that the hydrolysis of species containing nitrogen should lead to negative peaks in the region of 1650–1200 cm^{-1} in ATR-IR spectra. However, this was not

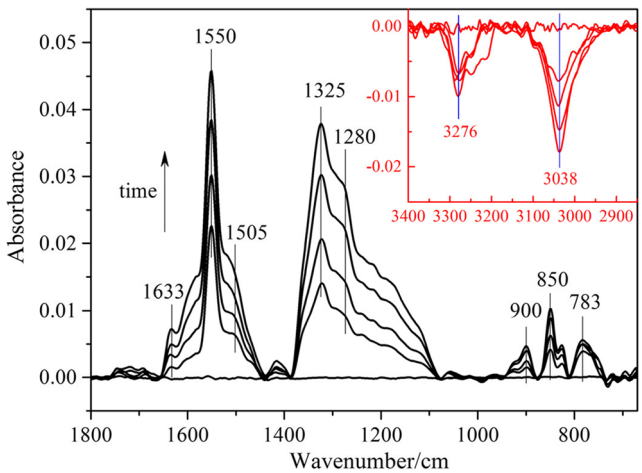

Fig. 4 Temporal changes of in situ ATR-IR spectra of "fuel-rich" soot during the reaction with NO_2 (5 ppm) at RH = 7%. The illustration in the upper right corner is the IR spectra in the range of 3400–2800 cm^{-1}

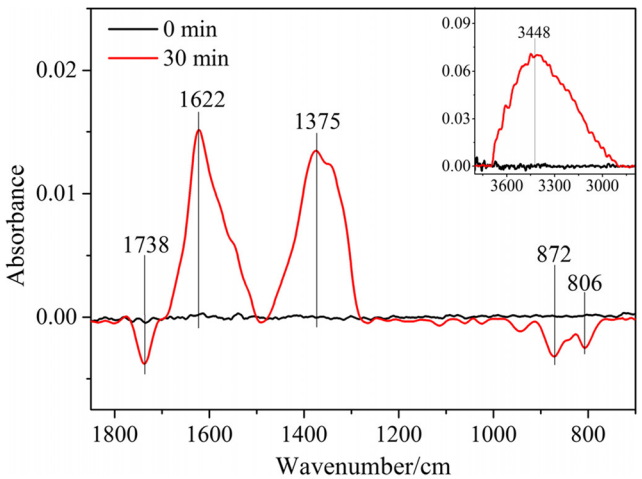

Fig. 5 IR spectra of "fuel-rich" soot aged by NO_2 (5 ppm) after being exposed to wet N_2 flow (RH = 70%). The illustration in the upper right corner is the IR spectra in the range of 3800–2800 cm^{-1}

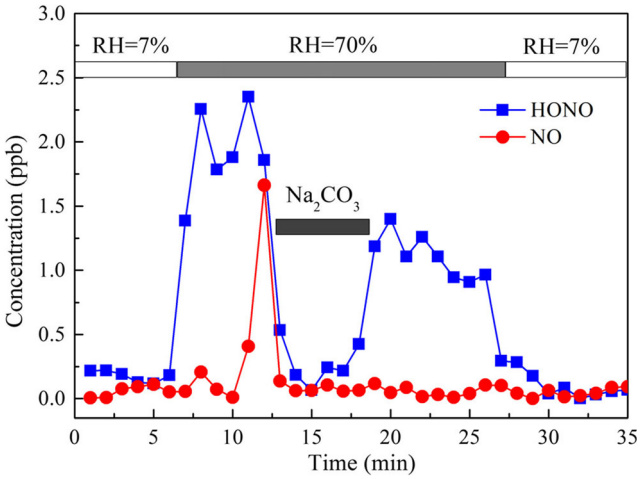

Fig. 6 Gaseous products during the exposure of "fuel-rich" soot aged by NO_2 (160 ppb) to the N_2 flow at RH = 7 or 70%

observed due to the offset caused by the adsorption peaks of H_2O and carboxylic species or alcohols.

To determine whether high RH plays an enhancement role in the release of HONO on aged soot by NO_2 (160 ppb), the surface of NO_2-aged soot was first purged by a relative dry N_2 (7% RH). When the NO_2 and NO concentrations were constant, a wet N_2 flow (70% RH) was introduced. As shown in Fig. 6, the red circles and blue grids represented the NO and NO_2 signals, respectively. When the carbonate tube was switched into the sampling line, it was proved that the NO_2 signal should be ascribed to HONO. The formation of NO had a delay and only persisted for 1–2 min. Upon exposing the aged soot to wet N_2, HONO was continuously generated. According to Fig. 5, HONO may originate from the hydrolysis of species containing nitrogen on soot. It has been reported that the hydrolysis of organic nitrites (RONO) can produce HONO (Allen 1953; Iglesias and Casado 2002). On the other hand, that H_2O can occupy adsorptive sites at high RH, leading to the release of adsorbed HONO produced by the reaction of NO_2 with soot, which should be a more reasonable explanation (Syomin and Finlayson-Pitts 2003). Figure 6 displays that the integrated HONO amount was about 7×10^{10} molecules cm^{-2} min^{-1}, which was two orders of magnitude less than that from the direct reaction of NO_2 with soot (Fig. 1). Therefore, the HONO yield within first 90 min range at RH = 70% seemed to be unchanged in comparison with that at lower RH (Fig. 2b). It should be noticed that if this HONO release can be always observed over a longer time scale, its integral amount may result in an increase of overall HONO yield.

Conclusions

The $\gamma_{initial}$ of NO_2 on soot exhibited a significant decrease at RH = 7–70%. For fuel-rich and fuel-lean soot, the $\gamma_{initial}$ at RH = 7% was $(2.59 \pm 0.20) \times 10^{-5}$ and $(5.92 \pm 0.34) \times 10^{-6}$, respectively, while the corresponding one was $(5.49 \pm 0.83) \times 10^{-6}$ and $(7.16 \pm 0.73) \times 10^{-7}$ at RH = 70%, respectively. The HONO yield remained unchanged as RH increased, and its average value was (72 ± 3)% and (60 ± 2)% for fuel-rich and fuel-lean soot, respectively. The Langmuir-Hinshelwood mechanism can explain the negative influence of an increasing RH on $\gamma_{initial}$, which was ascribed to the competitive adsorption of H_2O on soot. On the basis of in situ ATR-IR spectra, the reaction of NO_2 with soot produced various species containing nitrogen on soot including R-ONO, R-NO_2, and R-ONO_2, with the consumption of alkyne and aromatic compounds. The hydrolysis of species containing nitrogen may occur at high RH, followed by the generation of carboxylic species or alcohols and the release of little HONO and NO.

Acknowledgements This research was financially supported by the Strategic Priority Research Program of the Chinese Academy of Sciences (XDB05010301) and National Natural Science Foundation of China (21407020, 21190054, 91543109).

References

Akhter MS, Chughtai AR, Smith DM (1984) Reaction of hexane soot with NO_2/N_2O_4. J Phys Chem 88:5334–5342

Al-Abadleh HA, Grassian VH (2000) Heterogeneous reaction of NO_2 on hexane soot: a Knudsen cell and FT-IR study. J Phys Chem A 104: 11926–11933

Allen AD (1953) Hydrolysis of organic nitrites. Nature 172:301–302

Ammann M, Kalberer M, Jost DT, Tobler L, Rössler E, Piguet D, Gäggeler HW, Baltensperger U (1998) Heterogeneous production of nitrous acid on soot in polluted air masses. Nature 395:157–160

Arens F, Gutzwiller L, Baltensperger U, Gäggeler HW, Ammann M (2001) Heterogeneous reaction of NO_2 on diesel soot particles. Environ Sci Technol 35:2191–2199

Aubin DG, Abbatt JPD (2007) Interaction of NO_2 with hydrocarbon soot: focus on HONO yield, surface modification, and mechanism. J Phys Chem A 111:6263–6273

Bertram AK, Ivanov AV, Hunter M, Molina LT, Molina MJ (2001) The reaction probability of OH on organic surfaces of tropospheric interest. J Phys Chem A 105:9415–9421

Cain JP, Gassman PL, Wang H, Laskin A (2010) Micro-FTIR study of soot chemical composition—evidence of aliphatic hydrocarbons on nascent soot surfaces. Phys Chem Chem Phys 12:5206–5218

Cooney DO, Kim SS, Davis EJ (1974) Analyses of mass transfer in hemodialyzers for laminar blood flow and homogeneous dialysate. Chem Eng Sci 29:1731–1738

Daly HM, Horn AB (2009) Heterogeneous chemistry of toluene, kerosene and diesel soots. Phys Chem Chem Phys 11:1069–1076

Finlayson-Pitts BJ, Wingen LM, Sumner AL, Syomin D, Ramazan KA (2003) The heterogeneous hydrolysis of NO_2 in laboratory systems and in outdoor and indoor atmospheres: an integrated mechanism. Phys Chem Chem Phys 5:223–242

Gerecke A, Thielmann A, Gutzwiller L, Rossi MJ (1998) The chemical kinetics of HONO formation resulting from heterogeneous interaction of NO_2 with flame soot. Geophys Res Lett 25:2453–2456

Han C, Liu Y, Liu C, Ma J, He H (2012a) Influence of combustion conditions on hydrophilic properties and microstructure of flame soot. J Phys Chem A 116:4129–4136

Han C, Liu Y, Ma J, He H (2012b) Key role of organic carbon in the sunlight-enhanced atmospheric aging of soot by O_2. Proc Natl Acad Sci U S A 109:21250–21255

Han C, Liu Y, He H (2013a) Heterogeneous photochemical aging of soot by NO_2 under simulated sunlight. Atmos Environ 64:270–276

Han C, Liu Y, He H (2013b) Role of organic carbon in heterogeneous reaction of NO_2 with soot. Environ Sci Technol 47:3174–3181

Hueglin C, Gehrig R, Baltensperger U, Gysel M, Monn C, Vonmont H (2005) Chemical characterisation of PM2.5, PM10 and coarse particles at urban, near-city and rural sites in Switzerland. Atmos Environ 39:637–651

Iglesias E, Casado J (2002) Mechanisms of hydrolysis and nitrosation reactions of alkyl nitrites in various media. Int Rev Phys Chem 21:37–74

Kalberer M, Ammann M, Arens F, Gäggeler HW, Baltensperger U (1999a) Heterogeneous formation of nitrous acid (HONO) on soot aerosol particles. J Geophys Res Atmos 104:13825–13832

Kalberer M, Ammann M, Gäggeler HW, Baltensperger U (1999b) Adsorption of NO_2 on carbon aerosol particles in the low ppb range. Atmos Environ 33:2815–2822

Khalizov AF, Cruz-Quinones M, Zhang R (2010) Heterogeneous reaction of NO_2 on fresh and coated soot surfaces. J Phys Chem A 114:7516–7524

Kirchner U, Scheer V, Vogt R (2000) FTIR spectroscopic investigation of the mechanism and kinetics of the heterogeneous reactions of NO_2 and HNO_3 with soot. J Phys Chem A 104:8908–8915

Kleffmann J, Wiesen P (2005) Heterogeneous conversion of NO_2 and NO on HNO_3 treated soot surfaces: atmospheric implications. Atmos Chem Phys 5:77–83

Kleffmann J, Becker KH, Lackhoff M, Wiesen P (1999) Heterogeneous conversion of NO_2 on carbonaceous surfaces. Phys Chem Chem Phys 1:5443–5450

Lelièvre S, Bedjanian Y, Pouvesle N, Delfau JL, Vovelle C, Bras GL (2004a) Heterogeneous reaction of ozone with hydrocarbon flame soot. Phys Chem Chem Phys 6:1181–1191

Lelièvre S, Bedjanian Y, Laverdet G, Bras GL (2004b) Heterogeneous reaction of NO_2 with hydrocarbon flame soot. J Phys Chem A 108: 10807–10817

Liu Y, Han C, Ma J, Bao X, He H (2015) Influence of relative humidity on heterogeneous kinetics of NO_2 on kaolin and hematite. Phys Chem Chem Phys 17:19424–19431

Ma X, Zangmeister CD, Gigault J, Mulholland GW, Zachariah MR (2013) Soot aggregate restructuring during water processing. J Aerosol Sci 66:209–219

Martin M, Tritscher T, Jurányi Z, Heringa MF, Sierau B, Weingartner E, Chirico R, Gysel M, Prév t ASH, Baltensperger U, Lohmann U (2013) Hygroscopic properties of fresh and aged wood burning particles. J Aerosol Sci 56:15–29

McCabe J, Abbatt JPD (2009) Heterogeneous loss of gas-phase ozone on n-hexane soot surfaces: similar kinetics to loss on other chemically unsaturated solid surfaces. J Phys Chem C 113:2120–2127

Mikhailov EF, Vlasenko SS, Podgorny IA, Ramanathan V, Corrigan CE (2006) Optical properties of soot-water drop agglomerates: an experimental study. J Geophys Res Atmos 111:D07209

Monge ME, D'Anna B, Mazri L, Giroir-Fendler A, Ammann M, Donaldson DJ, George C (2010) Light changes the atmospheric reactivity of soot. Proc Natl Acad Sci U S A 107:6605–6609

Murphy DM, Fahey DW (1987) Mathematical treatment of the wall loss of a trace species in denuder and catalytic converter tubes. Anal Chem 59:2753–2759

Ndour M, Nicolas M, D'Anna B, Ka O, George C (2009) Photoreactivity of NO_2 on mineral dusts originating from different locations of the Sahara desert. Phys Chem Chem Phys 11:1312–1319

Penner JE, Eddleman H (1993) Towards the development of a global inventory for black carbon emissions. Atmos Environ 27:1277–1295

Popovicheva O, Persiantseva NM, Shonija NK, DeMott P, Koehler K, Petters M, Kreidenweis S, Tishkova V, Demirdjian B, Suzanne J (2008) Water interaction with hydrophobic and hydrophilic soot particles. Phys Chem Chem Phys 10:2332–2344

Prince AP, Wade JL, Grassian VH, Kleiber PD, Young MA (2002) Heterogeneous reactions of soot aerosols with nitrogen dioxide and nitric acid: atmospheric chamber and Knudsen cell studies. Atmos Environ 36:5729–5740

Saathoff H, Naumann KH, Riemer N, Kamm S, Möhler O, Schurath U, Vogel H, Vogel B (2001) The loss of NO_2, HNO_3, NO_3/N_2O_5, and $HO_2/HOONO_2$ on soot aerosol: a chamber and modeling study. Geophys Res Lett 28:1957–1960

Salgado Muñoz MS, Rossi MJ (2002) Heterogeneous reactions of HNO_3 with flame soot generated under different combustion conditions. Reaction mechanism and kinetics. Phys Chem Chem Phys 4: 5110–5118

Seisel S, Lian Y, Keil T, Trukhin ME, Zellner R (2004) Kinetics of the interaction of water vapour with mineral dust and soot surfaces at T=298 K. Phys Chem Chem Phys 6:1926–1932

Sosedova Y, Rouvière A, Bartels-Rausch T, Ammann M (2011) UVA/Vis-induced nitrous acid formation on polyphenolic films exposed to gaseous NO_2. Photochem Photobiol Sci 10:1680–1690

Stadler D, Rossi MJ (2000) The reactivity of NO_2 and HONO on flame soot at ambient temperature: the influence of combustion conditions. Phys Chem Chem Phys 2:5420–5429

Syomin DA, Finlayson-Pitts BJ (2003) HONO decomposition on borosilicate glass surfaces: implications for environmental chamber studies and field experiments. Phys Chem Chem Phys 5:5236–5242

Wehner B, Wiedensohler A (2003) Long term measurements of submicrometer urban aerosols: statistical analysis for correlations with meteorological conditions and trace gases. Atmos Chem Phys 3:867–879

Zelenay V, Monge ME, D'Anna B, George C, Styler SA, Huthwelker T, Ammann M (2011) Increased steady state uptake of ozone on soot due to UV/Vis radiation. J Geophys Res Atmos 116:D11301

Zhang D, Zhang R (2005) Laboratory investigation of heterogeneous interaction of sulfuric acid with soot. Environ Sci Technol 39: 5722–5728